Electron mobility variations in surface-charged indium tin oxide thin films

S. Dasgupta,[*] M. Lukas, K. Dössel, R. Kruk, and H. Hahn

Institute for Nanotechnology, Forschungszentrum Karlsruhe GmbH, P.O. Box 3640, D-76021 Karlsruhe, Germany
(Received 11 May 2009; revised manuscript received 23 July 2009; published 24 August 2009)

A large variation in electrical resistance induced by an electrochemical surface charge is observed for the ultrathin films of indium tin oxide (ITO). A decrease and increase in resistance is noticed when the negative and positive surface charge is applied to the ITO thin films, respectively. An increase in total effect-size is obtained with a decrease in film thickness. Two contributions are considered to account for the measured effect: the variation in the carrier density and the modification of the charge carrier mobility. The first contribution, which is estimated from the Hall-effect measurements and applied surface charge density, can explain only a small fraction of the observed variation in electronic transport. The correlation of the other contribution (i.e., a variation in the electron mobility) with the film morphology and the local electronic states is examined by scanning tunneling microscopy and spectroscopy studies. Scanning tunneling spectra suggest that a local variation in charge carrier density exists on the grain surfaces and at the grain boundaries. Upon electrochemical surface charging, this local variation in density of states should result in an increase in the electronic roughness of the surface and a deeper penetration of the applied electric field at the grain boundaries. Thus, it is considered that a pronounced surface and grain boundary scattering of the conducting electrons is responsible for the large (electric) field effect observed in highly conducting oxides such as ITO.

I. INTRODUCTION

Field-effect devices have redefined human life over the last fifty years with their countless new applications. However, such devices, which exhibit reversible changes in their macroscopic properties controlled via an external potential, are generally restricted to materials with low-carrier density, such as semiconductors,[1] piezoelectrics,[2] conducting polymers,[3] and nanotubes.[4] In bulk metals and/or highly conducting oxides the large charge carrier concentration limits the screening length (δ) of the external field to one[5] or few monolayers.[6,7] Consequently, in conventional material structures this results in an insufficient change in macroscopic properties to be measured experimentally and utilized for practical purposes. However, recently Gleiter *et al.*[8,9] have suggested that a measurable change in physical properties may be possible for highly conducting systems using nanometer-sized structures with very high surface-to-volume ratio and large surface charge density applied using electrochemical gating. For a nanoparticulate, nanoporous material under study, the advantages of using electrolytes over the gate dielectrics are: the orders of magnitude higher charge density/local field can be applied, and an electrolyte can easily penetrate all the open porosity of a nanoparticulate structure to apply a high-density surface charge on all nanoparticle surfaces. Following the initial idea given by Gleiter *et al.*, a change in resistance of a few percent has been achieved for gold thin films,[10] nanoporous gold,[11] and platinum compacts.[12] However, a much larger effect can be expected in conducting systems with carrier concentrations lower than in a pure metal, for example in conducting oxides. Along this line, the resistance variation upon electrochemical surface charging of a nanoporous nanoparticulate aggregate consisting of indium tin oxide (ITO) nanoparticles was examined recently.[13] As anticipated, a much larger change (more than three orders of magnitude change in resistance) in the transport properties has been observed for the nanoparticulate ITO aggregate in comparison to the pure metallic systems.

Subsequently, it has been suggested that such devices which are entirely solution processed, easy to fabricate, and inexpensive are of importance for printable electronics, as some of the major limitations of both organic and inorganic semiconductors are overcome.[13,14] However, a change in electrical resistance of such an extent is quite surprising for ITO as it is a degenerately doped semiconductor with typical metal-like electronic transport[15–17] and carrier concentration (n) ranging 10^{20}–10^{21} cm^{-3}. It has been tentatively assumed in our previous report[13] that the tiny necks between the nanoparticles with an average diameter of 15 nm are affected most by the external field and, hence, play the key role in the resistance modulation. Such highly conducting channel field-effect devices can be of potential interest in the field of electronics; hence, the present work aims to obtain a quantitative understanding of the external field-induced electronic transport in conducting oxide nanostructures.

The surface-charge-induced variation in electronic transport originates from two major contributions: (a) an induced change in carrier concentration, (b) a change in scattering cross-section, i.e., mobility of the charge carriers. However, in pure metals, the former contribution is found to explain majority of the effect.[10–12] For ITO, a larger screening length is expected compared to a metal like gold due to lower charge carrier density. Hence, a more pronounced effect from the later contribution, i.e., the field-induced modification of the electron scattering may be anticipated. Furthermore, the specific surface charge density of a charged ITO electrode is found considerably lower than for metals, due to the lower double layer capacitance (DLC) of the oxide. Hence, in case of the nanoparticulate, nanoporous ITO array the surface-charge controlled variation in carrier concentration is clearly not sufficient to account for the large change in electrical properties observed.[13] Therefore, in this report the well-defined geometry and the accurately controllable surface-to-volume ratio of the nanograined ITO thin films are exploited to elucidate the role of both contributions considered above. The advantages of thin films over the nanoparticulate, nano-
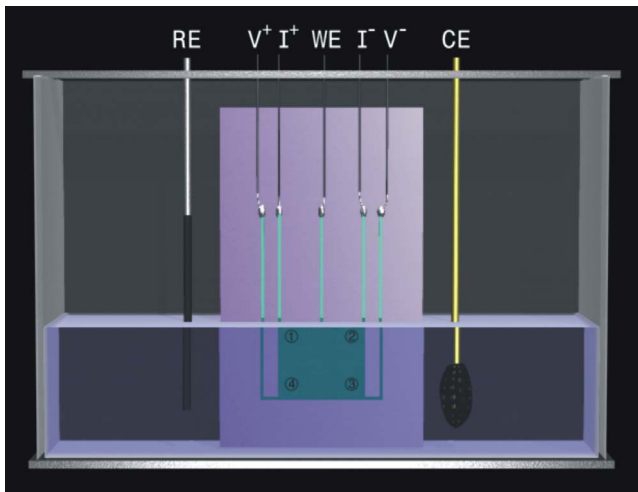
FIG. 1. (Color online) The electrochemical cell for the surface charge-induced resistance measurement including ITO thin film, (working electrode), Ag/AgCl reference electrode (RE), and amorphous carbon counter electrode (CE).

porous compacts are simpler geometry and the possibility to measure the surface area, surface-to-volume ratio and the specific surface charge density with high accuracy. In addition, the thin film geometry also facilitates the calculations of the other relevant parameters such as carrier concentration and the intrinsic carrier mobility.

II. EXPERIMENTAL

Thin films of indium tin oxide (In_2O_3 / SnO_2 $=90/10$ wt. %) were sputtered from a commercially available sputtering target (Kurt J. Lesker) at room temperature on thermally oxidized silicon wafers (Si/500 nm SiO_x) with 2.5 W/cm^2 sputtering power and 4.5×10^{-3} mbar Ar pressure. The base pressure of the system was less than 10^{-8} mbar. To improve the crystallinity the as-sputtered films were annealed in air for 2 h at 550 °C. A shadow mask was used to obtain the ITO thin films with van der Pauw geometry[18,19] (Fig. 1) suitable for four-probe resistance and Hall-effect measurements. x-ray reflectometry (XRR) and grazing incident x-ray diffraction (GIXRD) were carried out using a Bruker D8 diffractometer. Hall-effect measurements were performed using an extraction magnetometer (Quantum Design PPMS). Electrochemical measurements were carried out with an AUTOLAB PGSTAT 302 potentiostat in a conventional three-electrode setup. A solution of 0.1 M sodium perchlorate ($NaClO_4$) (Sigma-Aldrich) in propylene carbonate (Merck) was used as an electrolyte. High-surface area (>1000 m^2/g) activated carbon cloth (Kynol) and a freshly prepared Ag/AgCl electrode were used as the counter and reference electrode, respectively.

Scanning tunneling microscopy (STM) and spectroscopy (STS) measurements were performed on selected samples at room temperature. The samples were mounted into the ultra-high vacuum (UHV) system and annealed at the temperature of 120–150 °C to remove adsorbed water from the surface. The samples were then transferred to a modified Omicron
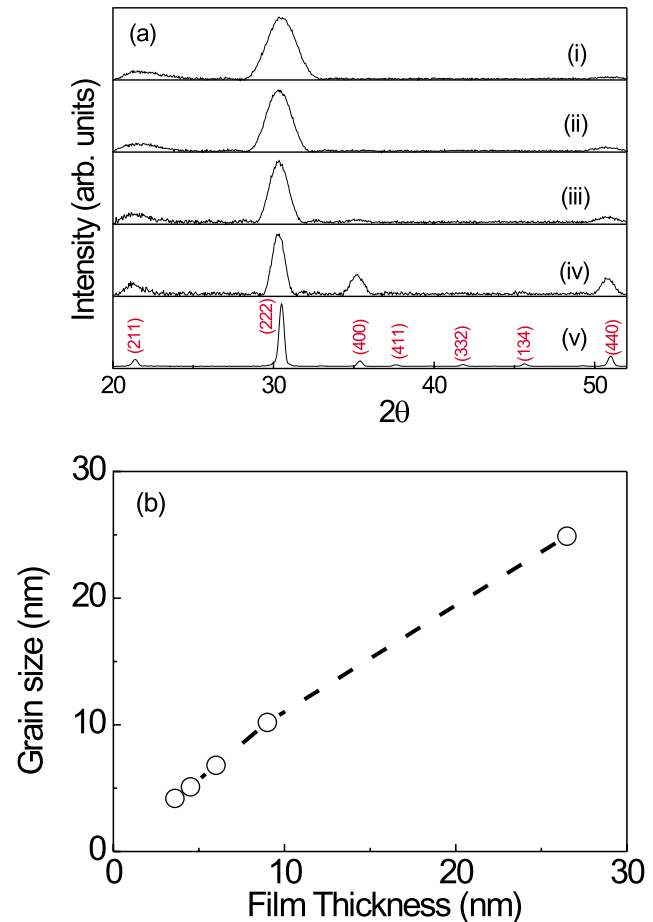
FIG. 2. (Color online) (a) The grazing incidence x-ray diffraction (GIXRD) patterns of the thin ITO films; plot (i)–(v) represent film thickness of 3.6, 4.5, 6, 9, and 26.5 nm respectively. (b) The film thickness plotted against calculated average grain size indicates equiaxed grains.

variable temperature UHV STM. All images shown were recorded in the constant current mode. In the STS mode, the tip was moved to the desired position and then the feedback was switched off to keep the sample-tip distance constant. The current was recorded while the voltage was ramped from zero to a maximum value of ± 3 V.

III. RESULTS AND DISCUSSION

The thickness of the sputtered and annealed ITO thin films, as determined through x-ray reflectometry, is 3.6, 4.5, 6, 9, and 26.5 nm, respectively. Figure 2(a) shows the GIXRD patterns of the films. The average grain diameter calculated using the classical Scherrer formula suggests equiaxed grains as the grain size is nearly equal to the film thickness [Fig. 2(b)]. The use of the Scherrer equation is justified since the microstrain is known to be negligible for air-annealed oxide thin films.[20]

The measurements of the surface charge-induced variation in sheet resistance of the ITO thin films were carried out with the electrochemical cell as shown in Fig. 1. The potential of the thin film was varied continuously with respect to
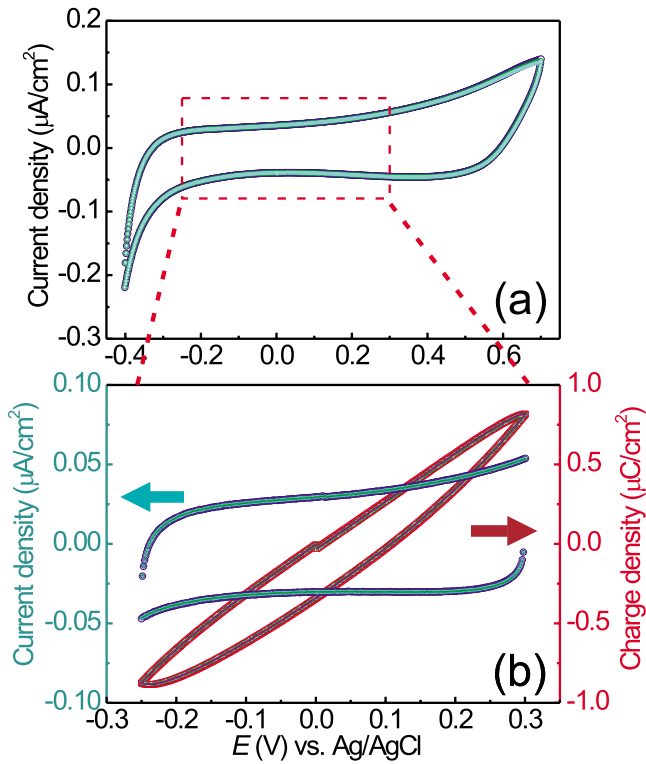
FIG. 3. (Color online) The cyclovoltammogram of the ITO thin film (3.6 nm) with a scan rate of 10^{-3} V s^{-1}: (a) Selection of the adsorption free predominantly double layer capacitive region, (b) The voltammetric cycles within the selected region (charging current corresponds to the left y axis) and also the surface charge density (right y axis) is shown. All the plots contain five complete potential scans.

the reference electrode. Simultaneously, the resistance of the film was measured passing a constant current. Therefore, this procedure is analogous to the measurement of channel conductance of a transistor with variation of the gate potential; so-called electrochemical gating.[13] To avoid chemical reactions at the ITO film/electrolyte interface, a careful selection of the adsorption-free, predominantly capacitive, potential region was necessary. This was achieved through a very slow (10^{-3} V s^{-1}) cyclovoltammetry. Cyclovoltammetry is a potentiodynamic electrochemical measurement in which the potential of the working electrode (ITO film in this case) with respect to the reference electrode is ramped at a constant rate (scan rate) versus time. After reaching the highest/lowest potential, the ramp direction is reversed. While a small constant current characterizes a capacitive region, a sudden increase in current is indicative of the onset of a chemical reaction. Figure 3(a) shows the cyclovoltammogram of the ITO thin film with the nominal thickness of 3.6 nm. From Fig. 3(a) the capacitive adsorption-free potential window from -0.25 V to 0.3 V (vs Ag/AgCl) was selected. Henceforth, for all the ITO films with different thickness, the potential was varied within this window. Figure 3(b) shows the cyclovoltammogram of the same sample within the desired potential region. The charge accumulated on the film surface was calculated by integrating the charging current. Simultaneously resistance measurements were performed us-
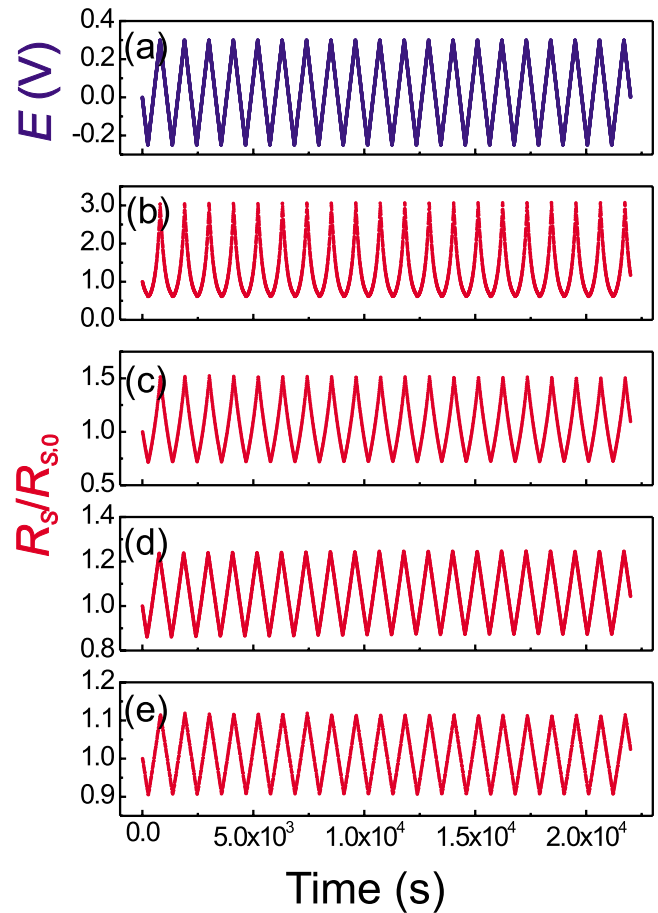
FIG. 4. (Color online) Change in the sheet resistance ($R_S/R_{S,0}$) of the ITO thin films. Figure 4(a) shows the gate potential variation with respect to the Ag/AgCl reference electrode. Figures 4(b)–4(e) show resistance modulation of the ITO films with film thickness of 3.6 nm, 4.5 nm, 6 nm, and 9 nm, respectively.

ing the van der Pauw method. A constant current of 10 μA was passed along one edge of the sample (for instance, I_{12}) and the voltage across the opposite edge (in that case, V_{43}) was measured (Fig. 1). To calculate the sheet resistance (R_S), the van der Pauw equation[18,19] was used:

$$R_S = \frac{\pi R_A}{\ln 2},\qquad(1)$$

where $R_A = \frac{V_{43}}{I_{12}}$. Figures 4(b)–4(e) shows the change in resistance of the ITO films with different thickness and, hence, different surface to volume ratios for the variation in the control potential [Fig. 4(a)]. It may be noted that all the measurements shown in Fig. 4 were initialized at the *open circuit potential* (OCP) of the thin films. The OCP was at *zero voltage* with respect to the Ag/AgCl reference electrode. Owing to the small build-in surface charge at OCP, the resistance of the films at zero voltage (denoted as $R_{S,0}$) was similar to that of the dry samples. In contrast, a large variation in resistance was observed when the electrode (thin film) potential was cycled within the potential window mentioned above. The resistance change ($R_S/R_{S,0}$) is found to increase with a decrease of the film thickness from 9 to 3.6 nm. This

is anticipated because the thinner the film is, the larger the surface to volume ratio is and, hence, higher the effect of surface charging. The highly reversible change in resistance [Fig. 4(b)–4(e)] furthermore ensures that the dominant reason for the resistance modulation is the electrostatic field effect and that the chemisorption is negligible within the selected potential window. It is also interesting to note a significant nonlinearity in the resistance variation observed only for the thinnest film (3.6 nm). Such a nonlinear variation in drain current is always observed in a transistor when plotted against the gate voltage.

The surface-charge induced large change in resistance of the thin ITO films can be analyzed by taking into account: (A) the variation in the carrier density with surface charging, (B) the modification of carrier mobility due to a change in scattering behavior upon charging.

(A) We may start with the classical Drude model[21] to account for the above mentioned counterparts:

$$\sigma = \frac{ne^2\tau}{m_e}, \tag{2}$$

where, σ is the conductivity, n is the charge carrier density, e is the elemental charge, τ is the relaxation time and m_e is the effective electron mass. Replacing relaxation time with charge carrier mobility, μ, one obtains:

$$\rho = (ne\mu)^{-1}, \tag{3}$$

where, ρ is the resistivity.

Hence, the resistance change can be expressed:

$$\frac{R_S}{R_{S,0}} = \left(\frac{n}{n_0} \times \frac{\mu}{\mu_0} \right)^{-1}, \tag{4}$$

where, n_0 and μ_0 are the initial charge carrier concentration and carrier mobility, respectively. To obtain the initial charge carrier concentration (n_0), Hall-effect measurements of the dry samples were performed. Figure 5 summarizes the results as a function of the film thickness. A gradual decrease in carrier concentration from $1.56 \times 10^{20}/\text{cm}^3$ to $6.7 \times 10^{19}/\text{cm}^3$ was observed with the decrease in film thickness from 9 nm to 3.6 nm. The measured resistivity (ρ_0) ($\rho_0 = R_{S,0} \times t$, t is the film thickness) and carrier density (n_0) allowed the calculation of carrier mobility (μ_0) and electron mean-free path (EMFP) (λ_0) for the dry samples.

EMFP can be calculated as:[21]

$$\lambda = \frac{m_e v_F \mu}{e} \tag{5}$$

and:

$$v_F = \frac{\hbar}{m_e}(3\pi^2 n)^{1/3}, \tag{6}$$

where v_F is the Fermi velocity and $\hbar$ is the reduced Planck's constant. The small values of the mean free paths, shown in Fig. 5(d), are characteristic of heavily doped semiconductors.[17] However, the pronounced scattering at the surfaces and grain boundaries are also limiting the EMFP in the ultrathin nanograined films. As can be seen from Fig. 5(d), a decrease in λ_0 is observed with a decrease in the film
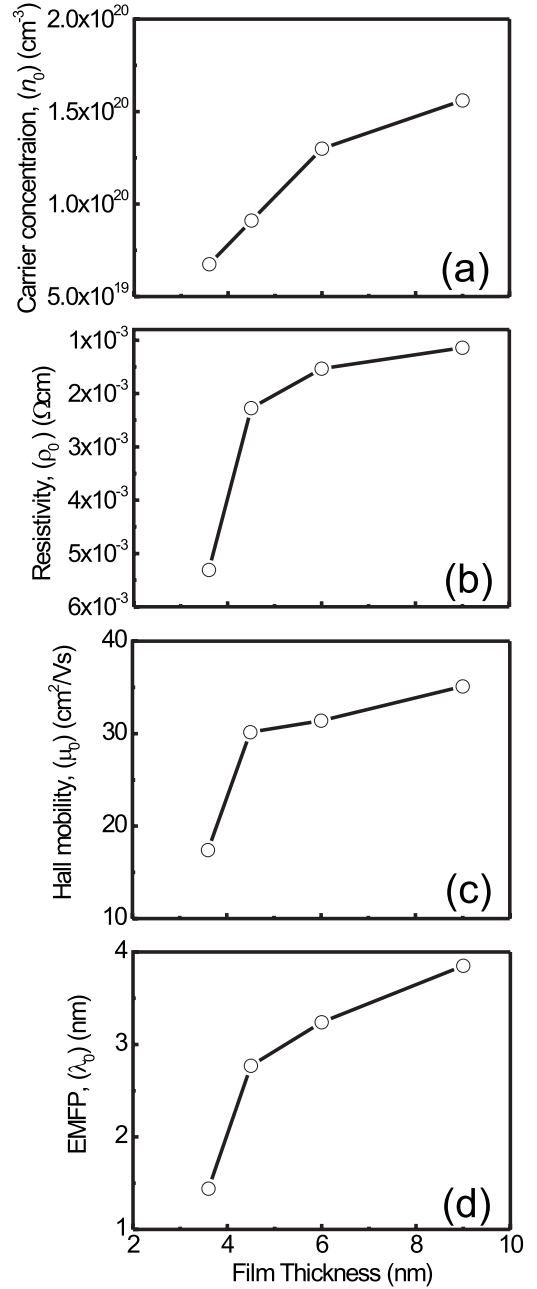
FIG. 5. Data obtained from sheet resistance and Hall-effect measurements performed on dry samples. The graphs show (a) carrier concentration, (b) resistivity, (c) Hall mobility, and (d) electron mean-free path, plotted versus film thickness.

thickness. The abrupt increase in resistivity for the thinnest film (3.6 nm) [Fig. 5(b)] is due to the abrupt decrease in carrier mobility/EMFP as can be seen from Figs. 5(c) and 5(d).

The carrier concentration in the charged thin films ($n = n_0 \pm \Delta n$) can be calculated knowing the initial carrier concentration (n_0) from the Hall-coefficient measurements, performed on the dry samples and the change in carrier concentration derived by integrating the charging current ($\Delta n = \Delta q/e$, Δq is the induced charge density) of the cyclovoltammograms. The underlying assumption is that all external charges are neutralized by the corresponding change in
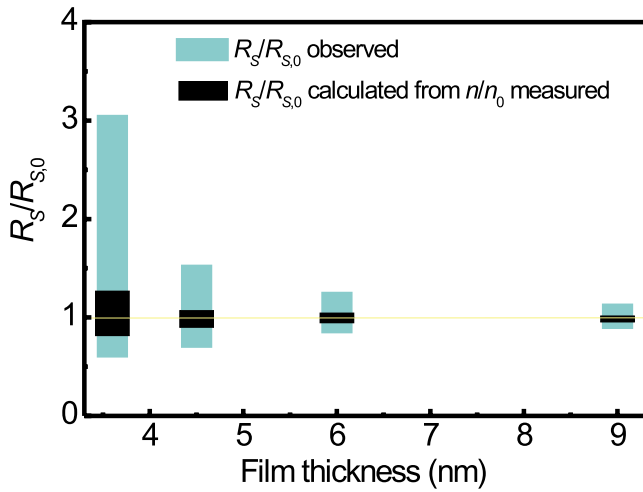
FIG. 6. (Color online) Comparison between the variations in the sheet resistance observed and calculated from the measured change in number of charge carriers.

FIG. 7. (Color online) Scanning tunneling microscopy images of ITO thin films with nominal thickness of (a) $t=3.6$ nm and (c) $t=9$ nm. The corrugation along the scan lines indicated in the images is shown in (b) and (d) for the two samples. The grains in both the samples can be easily seen.

charge carrier density in the film. This assumption is plausible as the potential window is completely in the double layer regime, without any adsorption and chemical reactions. The change in carrier concentration upon surface charging was calculated for all the films with different thickness using this approach. Under the assumption that the carrier mobility does not change with applied surface charge it is possible to compare the overall experimental change in resistance ($R_S/R_{S,0}$) to the change expected from the modification in free carrier concentration (n/n_0) (Fig. 6). It is evident from this comparison that only a small fraction of the resistance change can be explained by a change in carrier density. Hence, a large change in carrier mobility must be present.

(B) To consider the origin of the surface charge-induced modulation of the charge carrier mobility, the surface topography and the local density of states on the grains and at the grain boundaries need to be determined. Therefore, STM and STS studies were performed on selected samples. The STM images of the samples with a film thickness of 3.6 and 9 nm are shown in Figs. 7(a) and 7(c), respectively. Grain size and z corrugation of the samples are best seen in the line scans shown in Figs. 7(b) and 7(d). Apart from a plane or a sphere subtraction to compensate for the inclined mounting of the sample and the z-value artifacts of the single-tube piezoelectric scanner, the images are shown as recorded. The thinner (3.6 nm) sample shows a simple structure consisting of nearly round grains with a diameter of 2–5 nm, while the thicker one (9 nm) shows bigger grains and more irregular shape. Nevertheless a good agreement can be noticed between the grain size calculated from the x-ray line broadening and observed in the STM images. Additionally, the bigger grains show some fine substructure. It can be clearly seen that the grains in both samples in Figs. 7(a) and 7(c) are separated by half a nanometer deep trenches. In contrast, the substructures on the grain surfaces show much smaller height differences only in the range up to 0.1 nm. For the indium oxide lattice, the In-In, In-O, Sn-O atomic distances[22] are always larger than 0.2 nm, therefore these less than 0.1 nm height modulations within the grains is most likely due to
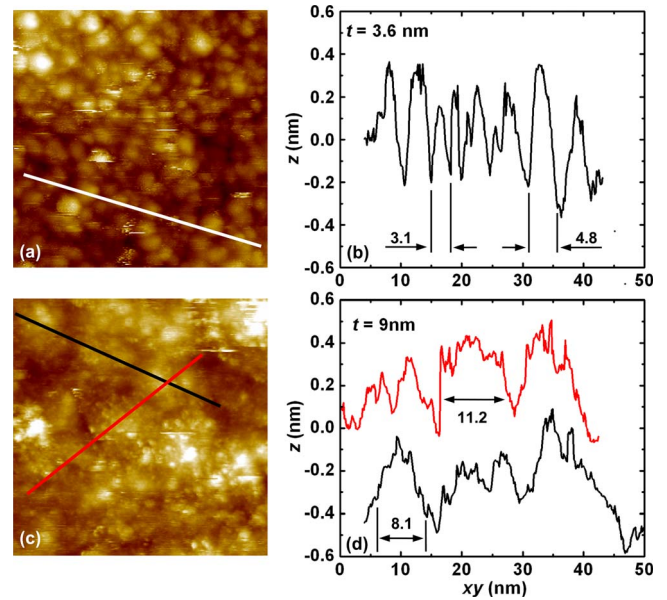
a local difference in the electronic states than due to the topography. At this point, it should be noted that the apparent height in the STM images recorded in constant current mode does not always reflect the real topographic surface features. A local increase (decrease) in the surface density of states gives rise to a higher (lower) tunneling current which induces the feedback loop of the STM to retract (approach closer with) the tip in order to keep a constant current. This movement of the tip is recorded as an apparent change in height.

To gain insight into the electronic properties of the surface, spectroscopic measurements on the grains and at the grain boundaries were performed. Measurements of the $I(V)$ curves for a positive and negative polarity were carried out separately. To ensure a better stability of the tip, the voltage was ramped from zero to either positive or negative values. The sample was biased with respect to the tip, which was grounded. Therefore, at positive voltage electrons were tunneling from the tip to the positively biased sample. An absence of data points around the Fermi level, $V=0$ V, (Fig. 8) is due to the smoothening procedure which requires several data points on either side to generate the averaged value. The measurements of $I(V)$ curves with a negative voltage below $V=-2.5$ V were possible for only a few times without obvious tip modifications induced by the voltage. Therefore, voltage values below -2.5 V were not further considered due to insufficient statistics. Finally, the conductance dI/dV was calculated numerically from the smoothened $I(V)$ data and normalized by I/V to obtain the logarithmic derivative $d \ln I/d \ln V=(dI/dV)/(I/V)$, which has been shown to be related to the surface density of states.[23] In order to extract the characteristic features of the density of states and eliminate artifacts, an averaging over many curves was performed.
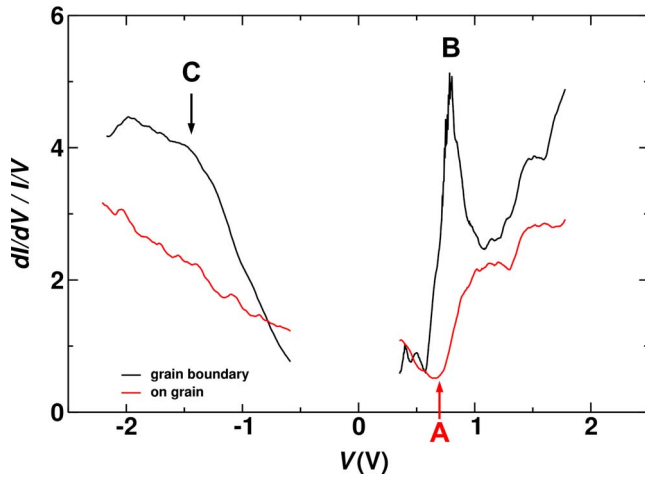
FIG. 8. (Color online) The normalized conductance, $d \ln I / d \ln V = (dI/dV)/(I/V)$, calculated from the scanning tunneling spectroscopy measurements on the grains and at the grain boundaries. The characteristic features are labeled A through C (see text).

About 20 $d \ln I / d \ln V$ curves per location and polarity of the applied voltage were added and then the spectra were averaged. These processed spectroscopic data are shown in Fig. 8.

A remarkable difference between the spectra taken on the grains and those measured at the grain boundaries is observed in agreement with Kasiviswanathan *et al.*[24] but in contrast to Matino *et al.*[25] The density of states observed on the grains resembles quite well the spectra recorded by Feenstra[23] for *n*-doped degenerated III–IV semiconductors. In degenerated, *n*-type semiconductors, the Fermi level E_F lies in the conduction band. Therefore, in absence of surface states one would expect a tunneling current occurring right away for $V > 0$. However, in degenerated ITO negatively charged surface states may exist.[26] The charge of these surface states has to be leveled off by a charge in the region below the surface, the so-called space charge. Therefore, the bands bend upward near the surface, bringing the conduction band above the Fermi level (Fig. 9). As a result, the usually filled and neutral donor levels become empty and hence positively charged. This depletion layer at E_F establishes a po-
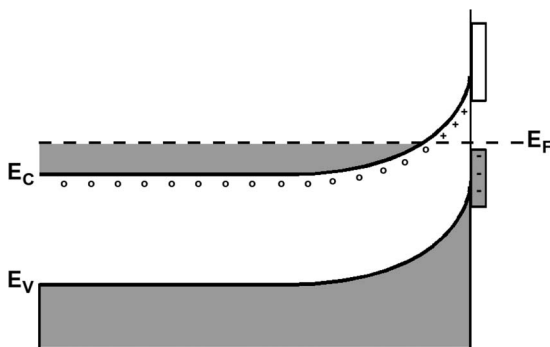
FIG. 9. Schematic diagram of the band structure of the ITO thin films. Band bending at the surface is due to the negatively charged acceptor-like surface states (shown as flat box) below E_F.

tential barrier for the electrons that tunnel from the surface through this depletion layer into the conduction band states in the bulk and thus reduces the tunneling probability right above E_F. Therefore, only a very weak tunneling current is found between $V = 0 - 0.5$ V. For the spectra taken on the grains an onset (point A) of conductance at 0.7 eV is seen which can be related to the conduction band edge. A similar band bending induced shift of the onset of conduction band was observed by Kasiviswanathan *et al.*[24] for nanograined ITO thin films. On the other hand, for the negative voltage, a monotonic increase in the density of states is observed. This conductance is attributed to the dopant levels which in case of a degenerate semiconductor are occupied and result in a small tunneling current at small negative voltages. This is denoted as a dopant-induced component in the literature.[23,25] The reported direct band gap of ITO derived from optical measurements is 3.75 eV.[27–29] Therefore, if the conduction band edge at the surface is at $V = 0.7$ eV, the surface valence band edge is expected to be at $V = -3.05$ eV. Therefore, the onset of the valence band was not recorded within the voltage range of the present measurements.

The spectra taken at the grain boundaries show a strong feature (peak) at the positive voltage (point B) in contrast to those taken on the grains. This feature can only be due to tunneling from the tip to the surface states (empty states) with a large DOS near the edge of the conduction band (Fig. 9). The presence of these surface states makes it difficult to determine the conduction band edge unambiguously: the onset may be somewhere around 1.1 eV. In agreement with the present results, Kasiviswanathan *et al.* also reported a shift in conduction band edge to a higher positive voltage for the spectra on the grain boundaries. An onset of the conduction band at the higher positive potential may result from a larger band bending induced by occupied, negatively charged, surface states. This is corroborated by the fact that the spectra on the grain boundaries show higher DOS at negative bias compared to the spectra on the grains. Therefore, beside the partly filled conduction band, additional occupied surface states must be contributing to the tunneling current. A broader depletion layer induced by a larger band bending may be the reason for the low conductance from 0 to −0.5 eV. The occupied states of the grain boundaries show a smeared out shoulder with a width of about 1 eV (marked C).

From the analysis of the STS spectra, it can be undoubtedly inferred that the spectra taken on the grain boundaries show more surface states (occupied as well as unoccupied) than those taken on the grains. It is believed that these large surface states result from the crystallographic as well as the compositional disorder such as a higher free volume, Sn segregation[30] and oxidation[22,31,32] near the grain boundaries. For instance, Gassenbauer *et al.*[26] have reported a direct relation between the surface states and the Sn concentration for the ITO thin films.

The excess amount of Sn and the oxygen content may be correlated: the higher Sn concentration leads to higher oxygen content in Sn rich phases. For the air-annealed ITO thin films, an increase in Sn concentration of up to 15 at.% near the grain boundaries compared to 5 at.% in the bulk was reported by Morikawa *et al.*[30] Since the solubility limit of Sn in In_2O_3 is around 6–9 at.%,[16,22,31–33] an excess of Sn leads

to phases such as SnO_2 or $In_4Sn_3O_{12}$.[22,31] The formation of intergranular amorphous phases with high concentration of neutral dopants was also reported.[32] Therefore, Sn segregation at the grain boundaries will bring the local Sn concentration above the solubility limit of Sn in In_2O_3 which would favor the oxygen rich phases locally. It has been observed that the presence of excess Sn and the oxygen-rich phases of Sn decreases the overall carrier concentration and conductivity of the bulk ITO.[22,31,32] The lowest conductivity in bulk ITO occurs at 6.5–10 at.% Sn concentration[34–38] which matches well with the reported solubility limit and is coherent with the model discussed here. It is expected that Sn segregation and oxidation at the grain boundaries decreases the local-carrier concentration and this should lead to a larger band bending.[39] Indeed, the onset of the conduction band was found to occur at a higher positive bias in the spectra taken on the grain boundaries compared to those on the grains.

Next, the possible relation of this local variation in the density of states with the large change in field-induced resistance will be considered. As can be seen from Figs. 7(b) and 7(d), a minor corrugation of the order of less than 0.1 nm was observed on the grain surfaces, which is believed to be due to a difference in the local electronic states. A local variation in the electronic states on the grains would lead to an inhomogeneous penetration of the electrostatic field applied at the surface. This in turn would make the film *electronically rougher*. This increase in electronic roughness of the surface should result in a decrease in specular (elastic) scattering of electrons at the surfaces. It is well known that a variation of surface specularity (P) may lead to a large change of carrier mobility and hence of resistivity.[40–42] Furthermore, from the above discussion it may be inferred that the Sn segregation leads to the grain boundary oxidation and consequently a decrease in carrier concentration at the grain boundaries. Hence, a positive field applied on the film surface would disrupt the conduction paths deeper at the grain boundaries. This would result in an enhanced grain boundary scattering. It can be concluded that in a heavily doped oxide conductor where the dopant segregation at the grain boundary leads to oxidation and in turn a decrease in number of carriers, the field-induced tunable modulation in the charge carrier mobility may cause a large field-effect which would not be observed otherwise.

To realize the extent of the tunable charge carrier mobility the thinnest film (3.6 nm) for which the resistance change is maximum is considered. With the positive surface charge (negative ions at the ITO interface) on the ITO surface, an increase in resistance by more than three times is observed. The decrease in mobility ($\mu = \mu_0 - \Delta\mu$) required to balance Eq. (4) can be calculated for this film. For the positively charged surface a decrease in carrier concentration of 5.12 $\times 10^{12}$ can be estimated from the integration of the charging current of the cyclovoltammogram in Fig. 3(b). Taking this decrease in carrier concentration into account, a decrease in carrier mobility from 17.4 to 7.6 $cm^2/V s$ is necessary to

explain the observed change in resistance. It is interesting to note that a more than twofold change of carrier mobility is achieved with the change of surface and grain boundary scattering due to the surface charge at the thin film/electrolyte interface.

Of course caution should be exercised when applying the free electron gas model to an electronically inhomogeneous system. If the grain boundaries are the high-resistive ligaments in the conducting film and the bulk transport is determined by the number of carriers and their mobility near the grain boundaries, then the electronic transport calculations should rather be carried out for the grain boundary regions only. A higher relative change in carrier concentration near the grain boundaries caused by the surface charge would result in a smaller change in mobility required to explain the observed effect. Nevertheless, the central conclusion still holds that an inhomogeneous field penetration, especially at the grain boundaries, is playing a decisive role in modulation of the bulk conductivity of ITO nanostructures.

IV. CONCLUSION

A large change in the sheet resistance with an electrostatic field applied at the surface is observed for nanograined, ultrathin indium tin oxide films. This phenomenon is remarkable for highly conducting ITO which is a degenerately doped semiconductor with carrier density higher than 10^{20} cm^{-3}. It is shown that a charge-induced variation in surface and grain boundary scattering of electrons is the major reason for the large field-effect observed. Spectroscopic study of the surface DOS supports the idea that the grain boundaries contain less charge carriers resulting in a deeper external-field penetration. The in-depth understanding offered in the present study elucidates the underlying basis of the large field-effect observed in the recently reported, solution processed (printable), transistor made from ITO nanoparticles. It has generally been observed with the heavily doped oxide conductors such as ITO, antimony tin oxide (ATO), doped ZnO, etc. that the dopant concentration close to the solubility limit offers the highest carrier concentration and hence the best electrical properties (lowest resistivity). Therefore, it may be a general tendency of such oxide conductors nanostructures (such as thin films, nanoparticles, and/or polycrystalline nanowires) that the dopant segregation and oxidation at the surface, near the grain boundaries or at the interparticle necks results in a local variation in density of states. Consequently, a large field effect in electronic transport results from a surface-charge controlled tunable electron mobility even though a considerable modulation in charge carrier density is not possible.

*subho.dasgupta@int.fzk.de

[1] S. M. Sze, *Physics of Semiconductor Devices*, 2nd ed. (Wiley, New York, 1981).

[2] J. F. Scott, Science **315**, 954 (2007).

[3] T. W. Kelley, P. F. Baude, C. Gerlach, D. E. Ender, D. Muyres, M. A. Haase, D. E. Vogel, and S. D. Theiss, Chem. Mater. **16**, 4413 (2004).

[4] V. N. Popov, Mater. Sci. Eng. R **43**, 61 (2004).

[5] K. Kempa, Surf. Sci. **157**, L323 (1985).

[6] K. P. Ghatak, A. K. Choudhury, S. Ghosh, and A. N. Chakravarti, Czech. J. Phys., Sect. B **30**, 925 (1980).

[7] T. Tošić, M. Jevtić, and D. Tjapkin, Univ. Beograd. Publ. Elektrotehn. Fak. Ser. Mat. Fiz. **634-677**, 148 (1979).

[8] H. Gleiter, Scr. Mater. **44**, 1161 (2001).

[9] H. Gleiter, J. Weissmüller, O. Wollersheim, and R. Würschum, Acta Mater. **49**, 737 (2001).

[10] S. Dasgupta, R. Kruk, D. Ebke, A. Hütten, C. Bansal, and H. Hahn, J. Appl. Phys. **104**, 103707 (2008).

[11] A. K. Mishra, C. Bansal, and H. Hahn, J. Appl. Phys. **103**, 094308 (2008).

[12] M. Sagmeister, U. Brossmann, S. Landgraf, and R. Würschum, Phys. Rev. Lett. **96**, 156601 (2006).

[13] S. Dasgupta, S. Gottschalk, R. Kruk, and H. Hahn, Nanotechnology **19**, 435203 (2008).

[14] S.-J. Hong, Y.-H. Kim, and J.-I. Han, IEEE Trans. Nanotechnol. **7**, 172 (2008).

[15] H. Odaka, Y. Shigesato, T. Murakami, and S. Iwata, Jpn. J. Appl. Phys. **40**, 3231 (2001).

[16] O. N. Mryasov and A. J. Freeman, Phys. Rev. B **64**, 233111 (2001).

[17] Z. Q. Li and J. J. Lin, J. Appl. Phys. **96**, 5918 (2004).

[18] L. J. van der Pauw, Philips Res. Rep. **13**, 1 (1958).

[19] L. J. van der Pauw, Philips Tech. Rev. **20**, 220 (1958).

[20] N. Audebrand, S. Raite, and D. Louër, Solid State Sci. **5**, 783 (2003).

[21] C. Kittel, *Introduction to Solid State Physics*, 7th ed. (Wiley, New York, 1996).

[22] N. Nadaud, N. Lequeux, and M. Nanot, J. Solid State Chem. **135**, 140 (1998).

[23] R. M. Feenstra, Phys. Rev. B **50**, 4561 (1994).

[24] S. Kasiviswanathan, V. Srinivas, A. K. Kar, B. K. Mathur, and K. L. Chopra, Solid State Commun. **101**, 831 (1997).

[25] F. Matino, L. Persano, V. Arima, D. Pisignano, R. I. R. Blyth, R. Cingolani, and R. Rinaldi, Phys. Rev. B **72**, 085437 (2005).

[26] Y. Gassenbauer, R. Schafranek, A. Klein, S. Zafeiratos, M. Hävecker, A. Knop-Gericke, and R. Schlögl, Phys. Rev. B **73**, 245312 (2006).

[27] R. N. Weiher and R. P. Ley, J. Appl. Phys. **37**, 299 (1966).

[28] C.-H. Yang, S.-C. Lee, T.-C. Lin, and S.-C. Chen, Thin Solid Films **516**, 1984 (2008).

[29] L. Gupta, A. Mansingh, and P. K. Srivastava, Thin Solid Films **176**, 33 (1989).

[30] H. Morikawa, H. Kurata, and M. Fujita, J. Electron Microsc. **49**, 67 (2000).

[31] H. Enoki, J. Echigoya, and H. Suto, J. Mater. Sci. **26**, 4110 (1991).

[32] R. Bel Hadj Tahar, T. Ban, Y. Ohya, and Y. Takahashi, J. Appl. Phys. **83**, 2139 (1998).

[33] G. Frank, L. Brock, and H. D. Bausen, J. Cryst. Growth **36**, 179 (1976).

[34] K. Nishio, T. Sei, and T. Tsuchiya, J. Mater. Sci. **31**, 1761 (1996).

[35] G. Frank and H. Köstlin, Appl. Phys. A: Mater. Sci. Process. **27**, 197 (1982).

[36] H. Köstlin, R. Jost, and W. Lems, Phys. Status Solidi A **29**, 87 (1975).

[37] O. P. Agnihotri, A. K. Sharma, B. K. Gupta, and R. Thangaraj, J. Phys. D **11**, 643 (1978).

[38] M. J. Alam and D. C. Cameron, Thin Solid Films **377-378**, 455 (2000).

[39] W. Mönch, *Semiconductor Surfaces and Interfaces*, 3rd ed., Springer Series in Surface Science Vol. 26 (Springer, Berlin, 2001).

[40] A. Berman and H. J. Juretschke, Appl. Phys. Lett. **18**, 417 (1971).

[41] E. C. McIrvine, Phys. Rev. **148**, 528 (1966).

[42] M. S. P. Lucas, J. Appl. Phys. **36**, 1632 (1965).